This article is published as part of the *Dalton Transactions* themed issue entitled:

Molecular Magnets

Guest Editor Euan Brechin
University of Edinburgh, UK

Published in issue 20, 2010 of *Dalton Transactions*

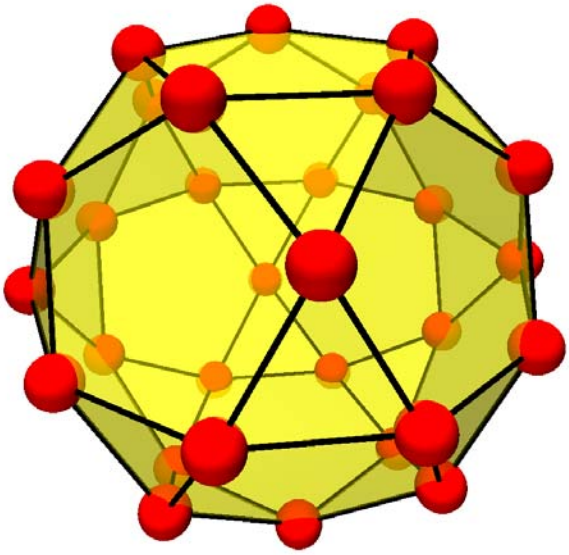

Image reproduced with permission of Jürgen Schnack

Articles in the issue include:

PERSPECTIVES:

COMMUNICATIONS:

Visit the *Dalton Transactions* website for more cutting-edge inorganic and organometallic research
www.rsc.org/dalton

Grafting molecular Cr_7Ni rings on a gold surface

Valdis Corradini,*[a] Alberto Ghirri,[a] Umberto del Pennino,[a,b] Roberto Biagi,[a,b] Victoria A. Milway,[c] Grigore Timco,[c] Floriana Tuna,[c] Richard E. P. Winpenny[d] and Marco Affronte[a,b]

Received 9th February 2010, Accepted 24th March 2010
First published as an Advance Article on the web 19th April 2010
DOI: 10.1039/c002425b

Molecular $\{Cr_7Ni\}$ rings have shown several ideal features for the observation of quantum phenomena and they appear suitable candidates for qubits encoding at low temperatures. We have exploited different functionalization pathways to graft molecular $\{Cr_7Ni\}$ rings onto a Au(111) surface from the liquid phase and here we report a comparative analysis of the results obtained by STM, XPS, XAS and XMCD experimental techniques.

Introduction

In order to fully exploit the functionalities of molecular nanomagnets (MNM) and, in particular, to use them as elementary units for high-density data storage[1–3] or for information processing, it is necessary to address the individual units. Binding them onto suitable substrates becomes a crucial step and, therefore, the design of appropriate derivatives and the implementation of procedures to attach molecules to surfaces need to be carefully addressed. Up to now, much effort has been devoted to studying the prototypical "single molecule magnet" Mn_{12} grafted onto surfaces using direct[4–6] and indirect deposition procedures.[7,8] Some other works have also shown successful deposition of magnetic systems on a surface (*e.g.* $TbPc_2$,[9,10] magnetic 2D networks,[11] spin transition systems[12]). Conversely, due to difficulties in finding suitable experimental techniques, only a few works have directly investigated the magnetic properties of sub-monolayers (sML) of such complex molecular systems[6,13] or nanoparticles.[14] Recent results have shown that the influence of the substrate, together with a high chemical reactivity and sensitivity to the X-rays, induces heavy changes in a sML of isolated Mn_{12} molecules on gold, thus compromising their magnetic behaviour.[5,6]

Here, we focus on $\{Cr_7Ni\}$ molecular antiferromagnetic rings, a new class of MNM in which interesting quantum phenomena have been observed[15–17] and that were recently proposed as candidates for the implementation of quantum gates.[18] $\{Cr_7Ni\}$ rings contain seven Cr^{3+} ions and one Ni^{2+} ion and their antiferromagnetic coupling leads to a molecular $S = 1/2$ spin ground state.[19,20] We have recently reported the design of sulfur-functionalized derivatives and the procedure to obtain, from liquid phase, sML distributions of such $\{Cr_7Ni\}$ rings grafted on Au(111).[20,21] We have also shown the influence of the surface on the properties of the grafted molecules with respect to the bulk.[22]

In the present work, we examined how the deposition procedures and the different functionalization pathways affect the chemical, electronic and magnetic properties of the grafted molecules. The investigation was carried out by means of scanning tunnel-microscopy (STM), X-ray photoemission spectroscopy (XPS), X-ray absorption spectroscopy (XAS) and magnetic circular dichroism (XMCD). In order to monitor the role of the sulfur based functionalization pathways in the grafting process, we have studied four $\{Cr_7Ni\}$ derivatives in which the number, location and orientation of the S groups is very different (amino-ethanethiol, thiophene, sulfur protected).

Besides this, we have also explored alternative routes for the deposition of the $\{Cr_7Ni\}$ rings on a Au(111) surface not exploiting the strong affinity between sulfur and gold. Namely we have studied $\{Cr_7Ni\}$ rings functionalized with polyaromatic ligands for which the grafting is secured by non-covalent interactions exploiting the affinity between the gold surface and a suitable organic group. In total we have studied seven $\{Cr_7Ni\}$ derivatives (four S-functionalized and three sulfur-free) in the form of microcrystalline thick films (TF), representative of the bulk, and sML distributions of isolated molecules deposited on Au(111). The investigated derivatives are: (**1**) Cr_7Ni-thio and (**2**) Cr_7Ni-thiobutane with a single alkanethiol attached to the central ammonium cation, (**3**) Cr_7Ni-3tpc with sixteen 3-thiophene-carboxylate ligands, (**4**) Cr_7Ni-4mtpp with one peripheric 3-4-methylthiophenyl-propionate (MTPP) ligand, (**5**) Cr_7Ni-pyridine with pyridinic ring (C_5H_4N) attached to the central ammonium cation, (**6**) Cr_7Ni-phenoxy, with 16 phenoxybenzoate ligands, (**7**) CoPc-Cr_7Ni where the Cr_7Ni ring is attached, through pyridine group, to the Co ion embedded in a phthalocyanine (CoPc).

Results and discussion

Derivatives with S ligands

The first two studied derivatives are the Cr_7Ni-thio $[HSC_2H_4NH_3][Cr_7NiF_8(O_2C^tBu)_{16}]$, (**1**) (see ref. 20) and Cr_7Ni-thiobutane $[HSCH_2CH_2NH_2^nBu][Cr_7NiF_8(O_2C^tBu)_{16}]$, (**2**) (see ref. 21), that show a single alkanethiol attached to the central ammonium cation. Unfortunately, the weak H-bond between the ring and the ammonium cation is broken in solution giving rise to the formation of a complete alkanethiol self-assembled monolayer (SAM). For both derivatives, the $\{Cr_7Ni\}$ surface coverage is relatively low (5–10%).We circumvented the weaknesses of the

[a]*CNR-Institute of NanoSciences, S3 via Campi 213/a, 41100, Modena, Italy. E-mail: valdis@unimore.it*
[b]*Dipartimento di Fisica, Università di Modena e Reggio Emilia, via Campi 213/a, 41100, Modena, Italy*
[c]*The Lewis Magnetism Laboratory, School of Chemistry, The University of Manchester, Oxford Road, Manchester, UK, M139PL*
[d]*The Photon Science Institute, The University of Manchester, Oxford Road, Manchester, UK, M139PL*

previous approach by transferring the bonding sulfur on a structure strongly linked to the ring. We started synthesizing the Cr_7Ni-3tpc [$^nPr_2NH_2$][Cr_7NiF_8(3-tpc)$_{16}$], (**3**) (see ref. 21) with sixteen 3-thiophenecarboxylate (TPC) ligands which present the S-atoms in the outer position of the thiophene ring. As expected, in this way the {Cr_7Ni} coverage increases significantly (15–30%). Although the TPC is more strongly bonded to the cluster core through Cr–O bonds, also in this case a significant tendency of the ligand to decompose becomes evident, leading to the formation of a SAM of thiophene on the surface. In order to avoid the competitive chemisorption of the clusters and of the SAM formed by the free ligands, we developed a {Cr_7Ni} derivative with sulfur ligands strongly bonded to the core, in which the affinity between S-species and the gold surface is strong enough to guarantee the grafting and where the sulfur-containing carboxylates are more stable. To this end we synthesized Cr_7Ni-4mtpp ([$(Et)_2NH_2$][$Cr_7NiF_8(O_2CCH_2{}^tBu)_{15}(O_2CCH_2CH_2C_6H_4SCH_3)$]
(**4**) see ref. 22) with one peripheric 3-4-methylthiophenyl-propionate ligand with a single protected S-atom. The coverage of this {Cr_7Ni} derivative is the highest we reached (20–35%) and, as expected, in this case we observed only a small quantity of free ligands in the first layer due to the small number of S-ligands broken in the solution.

STM of the S-derivatives

A two-dimensional (2D) distribution of {Cr_7Ni} derivatives on the Au(111) surface was obtained by liquid phase deposition. The four {Cr_7Ni} derivatives investigated and reported here contain S-groups able of establishing a chemical bond with the gold atoms of the surface. As mentioned in the previous section the number and orientation of these sulfur atoms is very different from one derivative to another (see right panels in Fig. 1). Different concentrations and different deposition times were exploited in order to find the best deposition conditions. The maximum coverage of clusters without the formation of 3D aggregates is obtained for concentrations in the range from 5–9 mM. Concerning the immersion times, we have found that the coverage does not significantly increase for immersions longer than 10 min up to 20 h. The result of each deposition process was monitored by means of the STM and XPS techniques. Typical STM imaging conditions were a bias voltages of 2.0 V and the lowest reachable tunnelling current (30 pA in our case), in order to minimize dragging and damaging of the organic materials by the scanning tip. The best conditions were reached immersing the Au(111) surface in a 5 mM solution of {Cr_7Ni} derivatives in THF for 10 min. The sample was then rinsed in THF and introduced into the UHV experimental chamber.

Room temperature STM images reported in Fig. 1 show for all systems the presence on the surface of an homogeneous 2D distribution of isolated {Cr_7Ni} clusters. There is no evidence of 3D aggregates (higher than 2 nm) and a small number of 2D aggregates with diameter larger than 5 nm. The low level of noise and the stability of the clusters even at high tunnelling currents (clusters are not shifted by the scanning tip up to 500 pA), confirm the strength of the molecule grafting on the Au surface. This is true not only for **1** and **2**, which are anchored with a single covalent S–Au bond, but also for **3**, where the grafting is secured by S atoms of the TPC ligands and for **4** where there is a single protected S atom

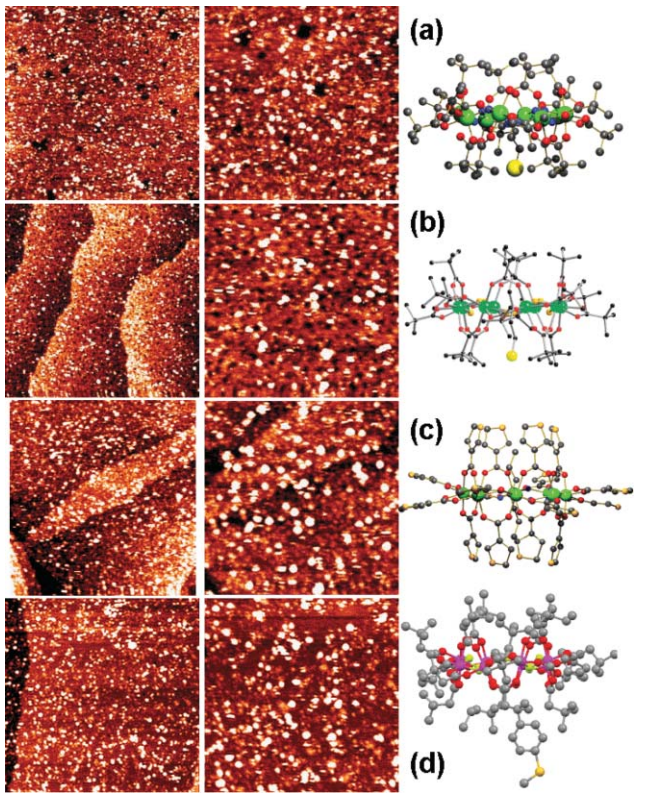

Fig. 1 Constant-current (30 pA, 2 V) STM images of the Au(111) surface immersed for 10 min in a 5 mM solution of the derivative **1** (a), **2** (b), **3** (c) and **4** (d): 200 × 200 nm^2 (left panel) and 100 × 100 nm^2 (central panel). The white entities represent the grafted clusters. In the right panel the structures of the **1**, **2**, **3** and **4** derivatives.

in the MTPP ligand interacting with the gold surface. In systems **1**, **2** and **3**, the black areas 2.4 Å deep (corresponding to the height of a monoatomic Au(111) step) and 5–10 nm wide, visible in Fig. 1a,b and c, indicate the formation of vacancy islands (VI).[21,24] The existence of the VI unambiguously reveals the presence of a first alkanethiol/TP SAM (detached from the outer shell of the ring) surrounding the clusters (see the sketch in Fig. 3), as also confirmed by XPS results. The kinetic of formation of the VI is very different from one derivative to another. For **1** and **2** we observe the VI formation after 10 min of immersion (see Fig. 1a,b) while for **3** the VI become more evident only for longer immersion times.[21] In **1** and **2**, the formation of a complete SAM[24,25] indicates that the bond between the ring and the ammonium-thiol is broken in solution. Despite the TPCs are expected to be strongly attached to the cluster core through Cr–O bonds, the formation of the SAM[26,27] indicates that also in **3**, a fraction of TP ligands dissociate in solution. The longer time required for the formation of densely packed TP SAM with respect to the alkanethiol may be explained by a lower mobility of the adsorbed TP molecules bonded to gold.[26] The situation is different in **4** where the absence of the VI and the presence of a low quantity of free ligands in the first layer (see Fig. 1d) suggest that only a small number of free ligands is in solution, as confirmed by XPS.

From the STM line-profiles (not shown) we can derive a diameter of 3.5 ± 0.5 nm for clusters **1**, **2** and **4** and a diameter of 4.0 ± 0.5 nm for **3**. This result is in agreement with the expected dimensions of the functionalized clusters (the ring diameter is

1.8 nm for **1**, **2** and **4** and 2.2 nm for **3**) convoluted with the curvature radius of the tip, assuming that the ring lay flat on the surface. The height of the clusters of **3** (1.0 ± 0.1 nm) is larger than for **1** and **2** (0.8 ± 0.1 nm). In both cases the height is lower than that expected for the clusters (1.5 nm and 1.1 nm respectively), confirming the presence of a first SAM of free alkanethiol \ TP ligands (about 0.5–0.6 nm height), which surrounds the clusters (see the sketch in Fig. 3). The situation is different in **4** where the SAM of free ligands is largely incomplete (Fig. 3, central panel), and the height of the clusters measured with respect to the surface (1.4 ± 0.1 nm) is comparable with the expected value (1.5 nm). A statistical analysis applied to the STM images (see Table 1) finds the most dense packing for **4**, with about 20–30% of the surface occupied by a 2D distribution of isolated clusters. The coverage is a bit lower for **3** (15–25%), while for **1-2** it is only 5–10%.

XPS of the S-derivatives

The STM results are confirmed by quantitative XPS investigations. In Fig. 2 the core levels of the Cr_7Ni/Au(111) interface obtained by immersing the gold surface in a 5 mM solution of **2**, **3** and **4** in THF for 10 min are compared (the spectra of **1** are omitted since they reproduce exactly those of **2**). Core level intensities have been normalized taking into account the atomic sensitivity and the attenuation of the electronic signal. The Cr 2p, F 1s and Ni 2p core level line-shapes measured for the MLs fit well with the corresponding data obtained for a multilayer deposited from liquid phase (see details in the Experimental), indicating that the ring stoichiometry is preserved. For every system, the F 1s/Cr 2p and Cr 2p/Ni 2p ratios are well reproducible and close to the expected ones (see Table 1), confirming the stability of the ring. At variance, the S/7Cr ratio (not reported in Table 1) indicates a significant excess of sulfur. The ratio S 2p/Au 4f suggests the presence of a sulfur-containing monolayer surrounding the clusters for all systems, in agreement with STM results. From the Au 4f/Cr 2p ratio and taking into account the gold signal attenuation due to the overlayer, we can derive the average area

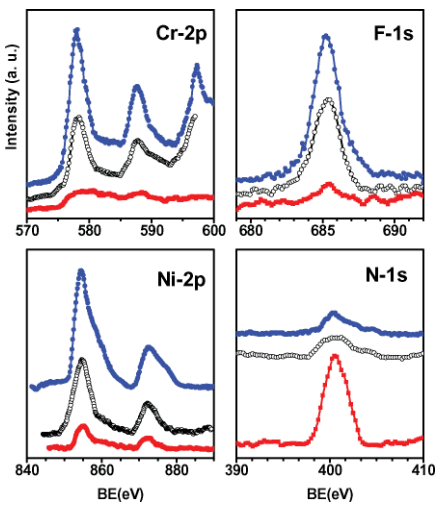

Fig. 2 Core level spectra obtained after immersing the Au(111) surface for 10 min in a 5 mM solution of **4** (upper spectra), **3** (central spectra) and **2** (lower spectra). The background contribution has been subtracted. In the Cr 2p energy region, the peak at high BE is the KLL Auger peak of F.

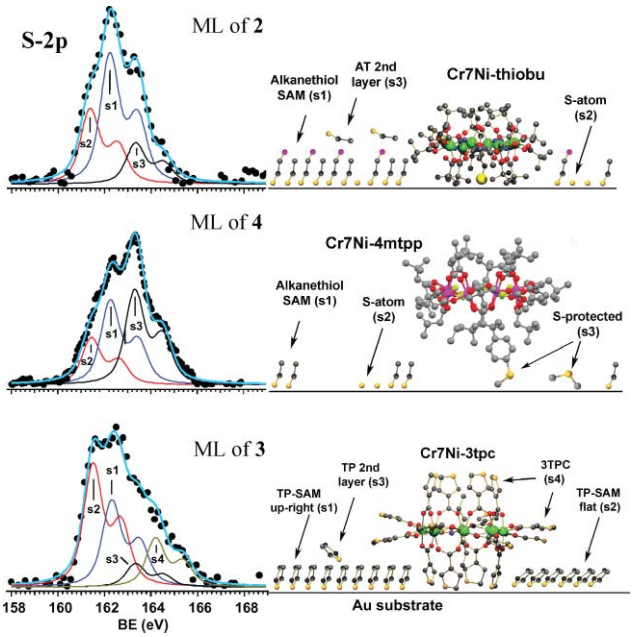

Fig. 3 Comparison between S 2p core level fits for ML of **2** (top panel), **4** (central panel) and **3** (bottom panel). The fitting parameters are reported in the text. In the right panel, a sketch of the situation: each cluster is surrounded by a SAM formed by free S-ligands as discussed in the text.

occupied by each cluster of 7–10 nm^2 per molecule in **4**, 12–18 nm^2 per molecule in **3** and of 28–44 nm^2 per molecule in **2**. Assuming that the complete coverage is made by molecules laying flat on the surface and considering an area of 2.5 nm^2 for clusters **1**, **2**, **4** and 3.8 nm^2 for **3**, we calculated the coverages, reported in Table 1, which are in good agreement with the values derived from STM. In addition to S 2p, also the N 1s stoichiometry is not respected: Nitrogen signal is much more intense for the ML's of **1** and **2** (see Fig. 2), indicating the presence of a SAM of free ammoniumthiols which break in solution. Conversely for ML's of **3** and **4**, the amina placed at the center of each Cr_7Ni ring is stable.

In order to further investigate the interface composition, we isolated the different contributions to the S 2p core level (see Fig. 3 and Table 1). The S 2p fitting procedure has been performed using spin–orbit-split doublet components (Voigt functions), with the following parameters: spin–orbit splitting of 1.2 eV, branching ratio of 0.5, Lorentzian width of 574 meV and Gaussian width of 600 meV for all components. The good quality of the fit (see Fig. 3) is also confirmed by the small values of the reduced χ^2 (2.2, 1.9 and 2.3 for the ML of **2**, **3** and **4**, respectively). For the ML's of **2** and **4** three components are observed at 161.4 eV (S2 peak), 162.2 eV (S1) and 163.3 eV (S3). S1 can be easily assigned to thiolate S atoms bonded to gold, while S3 to unbound S atoms,[28,29] due to the presence of a second layer of free alkanethiols in **2** and to the protected S-atom of the MTPP ligand in **4** (see the sketch of Fig. 3). The S2 component is usually assigned to isolated atomic S deriving from the C–S bond cleavage[30] or to a thiol bonded through sulfur, in an *sp* configuration.[29] In both cases the S2 component is associated with sulfur species bonded to gold. From the Au/(S1 + S2) ratio, we can derive for **2**, a packing level for the first S-monolayer of 23–31 $Å^2$ per sulphur atom suggesting the presence of a complete SAM of alkanethiols[25] (see Fig. 3 upper panel). Moreover, the S3/(S1 + S2) ratio indicates that about

Table 1 Stoichiometric ratios derived from the core level intensities of the derivatives **1**, **2**, **3** and **4** deposited on the Au(111) surface. The expected stoichiometric values are reported in brackets. Energy position and weight of the four components identified in the S 2p fitting procedure are discussed in the text. In the last two columns the Cr_7Ni coverage derived by XPS and STM are compared.

Derivative		F1s/Cr2p [1.14]	Cr2p/Ni2p [7]	S1-ev (%)	S2-ev (%)	S3-ev (%)	S4-ev (%)	S-SAM packing	XPS cover	STM cover
1	Cr_7Ni thio	1.13 ± 0.05	6 ± 2	162.2 (53%)	161.4 (30%)	163.3 (17%)	—	70–80%	10–20%	5–10%
2	Cr_7Ni thiobu	1.13 ± 0.05	5 ± 2	162.2 (53%)	161.4 (30%)	163.3 (17%)	—	80–90%	6–9%	5–10%
3	Cr_7Ni 3tpc	1.09 ± 0.05	6 ± 2	162.3 (31%)	161.5 (44%)	163.3 (8%)	164.2 (17%)	90–100%	20–30%	15–25%
4	Cr_7Ni 4mtpp	1.11 ± 0.05	6 ± 2	162.2 (38%)	161.4 (22%)	163.3 (40%)	—	20–30%	25–35%	20–30%

10–15% of the first SAM is covered by a second layer of unbound free alkanethiol ligands. For **4** instead, the Au/(S1 + S2) and Au/S3 ratios indicate that about 25% of the surface is covered by a first layer of sulfur species bonded to gold (see Table 1) and 15% by sulfur protected species like MTPP. Since the S3/7Cr 2p ratio is about 3 instead of 1, indicates that only 1/3 of these MTPP ligands is anchored to the Cr_7Ni core. For **3**, four components are observed at 161.5 eV (S2), 162.3 eV (S1), 163.3 eV (S3) and 164.2 eV (S4). S1 and S2 have been assigned to S atoms of thiophene molecules chemisorbed on gold in two different adsorption geometries.[26,27] TP ring could dissociate in solution due to the cleavage of one C–C bond.[31] In both cases (TP molecules in different adsorption geometries or alkyl-thiolate deriving from broken TP rings), S1 and S2 are associated with two sulfur species bonded to gold, while the S3 and S4 are assigned to unbound TP molecules which are not involved in the formation of the SAM.[27,29] Thus, the Au/(S1+S2) ratio indicates the presence of a complete SAM of sulfur species bonded to gold with a packing level (20–26 $Å^2$ per sulphur atom) slightly higher than in **2**. For each {Cr_7Ni} ring there are probably four TPC ligands bonded with gold through their sulfur atom and twelve with unbound S (see the sketch of Fig. 3). Since the ratio S4/Cr = 1.5 ± 0.2 is in reasonable agreement with the expected value of 1.7 (12/7), we can suppose that S4 can be attributed to unbound S of TPC ligands which are still linked to the cluster. S3 is then tentatively assigned to TPC ligands which are separated from the core of the cluster but where S is not bound to Au. From the S3/(S1 + S2) ratio, we derive that about 8% of the surface is covered by a second layer of unbound free TP ligand.

In summary, the combined STM-XPS analysis reveals that system **4**, with one peripheral MTPP ligand and a single protected S-atom, realizes the highest coverage showing also the smallest number of ligands broken in solution. The fact that we observe a SAM of free ligands does not means that the grafted rings have lost part of their functionalization. Indeed it is likely that for **1**, **2** and **4** where there is only one S-ligand for each molecule, we can safely suppose that the grafted rings preserve the S atom as evidenced by the stability of the clusters even at high tunnelling currents, which confirm the strength of the grafting with the Au surface. Thus we can suppose that the alkanethiols SAM is formed by ligands which break in solution from other molecules which are removed from the surface by the rinse. The only case in which the grafted ring could have lost part of their ligands is the **3** since it is functionalized with 16 TPC. If we suppose valid the attribution of the S4 component to unbound S of the TPC which are still linked to the cluster, the fact that the ratio S4/7Cr = 12 indicate that also in this case the cluster maintain the most part of the TPC ligands.

S-free derivatives

To corroborate the effectiveness of the S-functionalization, we also investigated the deposition of **5** *i.e.* Cr_7Ni-pyridine ($[PyCH_2NH_2Et][Cr_7NiF_8(O_2C^tBu)_{16}]$, Fig. 4a) with pyridinic functionalization in which the pyridinic ring (C_5H_4N) substitutes the SH termination of the (butylamino)ethanethiol.[32] In this case the STM images indicate that clusters are promptly removed by rinsing with the solvent, with a final coverage below 2% (see Fig. 4a). XPS experiments, reported in Table 2, confirm this outcome. The fact that clusters can easily be moved by the scanning tip, also at the

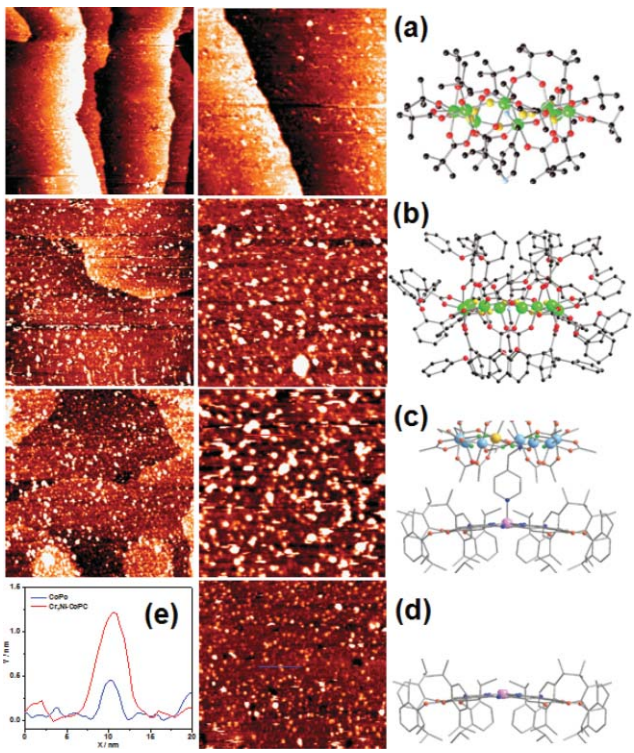

Fig. 4 Constant-current (30 pA, 2 V) STM images of the Au(111) surface immersed for 10 min in a 5 mM solution of the derivative **5** (a), **6** (b), **7** (c) and of the CoPc moiety (d): 200 × 200 nm^2 (left panel) 100 × 100 nm^2 (central panel). In the right panel the corresponding structures are shown. (e) Profiles measured along the lines drawn in panels (c) and (d).

Table 2 Stoichiometric ratios derived from the core level intensities of **5**, **6** and **7** deposited on the Au(111) surface. The expected stoichiometric values are reported in brackets. In columns 5 and 6, the number of CoPc for each Cr_7Ni and the CoPc coverage are shown. In the last two columns the Cr_7Ni coverages derived by XPS and STM are compared.

Derivative		F1s/Cr2p [1.14]	Cr2p/Ni2p [7]	N1s/Co2p [8+2]	Co2p/7Cr2p	CoPc Cover.	XPS cover	STM cover
5	Cr_7Ni pyrid	—	—	—	—	—	0–5%	<2%
6	Cr_7Ni phenoxy	1.12 ± 0.05	7 ± 2	—	—	—	20–30%	15–25%
7	CoPc-Cr_7Ni	1.15 ± 0.05	7 ± 2	10 ± 2	2.2	40–60%	15–25%	10–20%

lowest value of tunnelling current (30 pA), indicates that the rings are not immobilized on the gold surface. These findings prove that the three sulfur based functionalization pathways investigated (amino-ethanethiol, TPC and MTPP) effectively act to guarantee the stability of the grafting on the Au surface.

We have also explored routes alternative to the S–Au bond for the deposition from liquid phase of {Cr_7Ni} rings on Au(111) surface. Namely, we investigated the deposition of Cr_7Ni-phenoxy rings (see derivative **6** in Fig. 4b, $[^nPr_2NH_2][Cr_7NiF_8(O_2CC_6H_4OC_6H_5)_{16}]$) where the inner core is functionalized with poly-aromatic ligands (see ref. 22). Here the grafting on gold can be provided by non covalent interactions (π or Van der Waals). A more complex strategy that we have adopted exploits the high affinity of cobalt-phthalocyanines (CoPc) with the gold surface. The CoPc deposited on Au(111) forms ordered structures with molecules lying preferentially flat on the surface.[33] We have studied the deposition of CoPc-Cr_7Ni complexes[23] (derivative **7**, formula $C_{216}H_{301}N_{10}O_{40}F_8Cr_7NiCo$) whose structure is depicted in Fig. 4c. Here the {Cr_7Ni} ring is attached through a pyridine group to the Co^{2+} ion embedded inside the phthalocyanine.[23]

STM of the S-free derivatives

In Fig. 4 STM images, obtained after immersing the Au(111) surface in a 5 mM solution of the **6**, **7** derivatives and the CoPc moiety in DCM for 10 min, are shown. Also in this case, we observed the presence of an homogeneous 2D distribution of isolated {Cr_7Ni} clusters on the surface. A higher level of noise was present together with a reduced stability of the clusters with respect to higher tunnelling currents. The latter observation may indicate a weaker grafting of the molecules with respect to sulfur based derivatives. From the STM line-profiles (not shown), we can derive a diameter of 4.0 ± 0.5 nm and a height of 1.0 ± 0.1 nm for clusters **6** in agreement with the expected dimensions of this functionalized derivative. In **7** instead, two different kinds of entities can be identified (see Fig. 4c, 4e). Small spots, with dimensions (diameter = 2.5 ± 0.5 nm and height = 0.4 ± 0.1 nm) are comparable with those of the flat CoPc[33] (as shown in Fig. 4d), while bigger spots (diameter = 4.0 ± 0.5 nm and height = 1.3 ± 0.2 nm) correspond to the dimensions of {Cr_7Ni} clusters on top of the CoPc ML. From a statistical analysis of the STM images (see Tab. 2) we derive a coverage of about 15–25% for **6**, while for **7** about 10-20% of the surface was occupied by {Cr_7Ni} clusters and 40-50% by CoPc.

XPS of the S-free derivatives

The STM results are corroborated by quantitative XPS investigations. Also in this case the Cr 2p, F 1s, Ni 2p, Co 2p, N 1s, core levels line-shapes (spectra not shown here) taken on monolayer depositions are largely coincident with the spectra obtained for the corresponding multilayer. For every system, the ratios F 1s/Cr 2p and Cr 2p/Ni 2p are reproducible and close to the expected ones (see Tab. 2), indicating that the ring stoichiometry is preserved. The N 1s/Co 2p ratio is also reproducible every run, proving that the CoPc stoichiometry is preserved too. From the Au 4f/Cr 2p ratio, accounting for the signal attenuation due to the presence of the overlayer, we derived an average area occupied by each cluster of 15–22 nm^2 per molecule for **6** and of 10–17 nm^2 per molecule for **7**. The corresponding coverages for **6** (area of 4.5 nm^2) and **7** (area of 2.5 nm^2), reported in Tab. 2, are in good agreement with the values derived from STM. Moreover, from the Au 4f/Co 2p ratio we can derive that about 50% of the surface is covered by CoPc (see Tab. 2). Since the Co 2p/7Cr 2p ratio is about 2.2 instead of 1, we conclude that less than half of the CoPc's are still anchored to the {Cr_7Ni} ring and more than one half is free, again in good agreement with the STM.

XAS and XMCD

In this section we report results of our check of the chemical and magnetic properties of {Cr_7Ni} individual rings deposited on Au(111). In Fig. 5 the Cr and Ni $L_{2,3}$ XAS and XMCD spectra of the MLs of **3**, **4**, **6** and **7** (measured at 5 T and 10 K), are compared with the thick films (TFs) of **3** and of the pristine (not functionalized) Cr_7Ni-pivalate.[22,34] In all MLs and TFs, the XAS and XMCD spectral line shape are very similar (apart from the sign of the Ni dichroism that will be discussed below). The Cr absorption spectra present eight features characteristic of Cr^{3+} in O_h environment,[35] whereas the Ni XAS presents two peaks at the L_3 edge and a partially resolved doublet structure at the L_2 edge, characteristic of a high-spin Ni^{2+} ion in O_h environment.[36] Since the spectra of all the TFs perfectly reproduce those of **3**, we conclude that the different functionalization pathways do not affect the core electronic structure of the ring. In addition, Cr and Ni $L_{2,3}$ absorption spectra for all the MLs closely resemble those of the TFs. These results show that the grafting onto the gold surface does not affect the valence electronic structure of the Cr and Ni ions: namely oxidation state, local environment, and crystal-field intensity at the Cr and Ni sites are not altered by the deposition onto the surface.

XAS and XMCD spectra can be simulated by using the ligand field multiplet model implemented by Thole.[37,38] In ref. 22 we have calculated the $L_{2,3}$ absorption edges for the Ni^{2+} and Cr^{3+} ions as a function the crystal-field parameters (10Dq, Ds, and Dt). Strictly speaking, the local symmetry of both Ni^{2+} and Cr^{3+} ions should be tetragonal (D_{4h}), however we found a good agreement between the experimental spectra and theoretical simulations by considering the ions in O_h symmetry: Ds = Dt = 0, 10Dq = 2.1 eV for Cr^{3+}

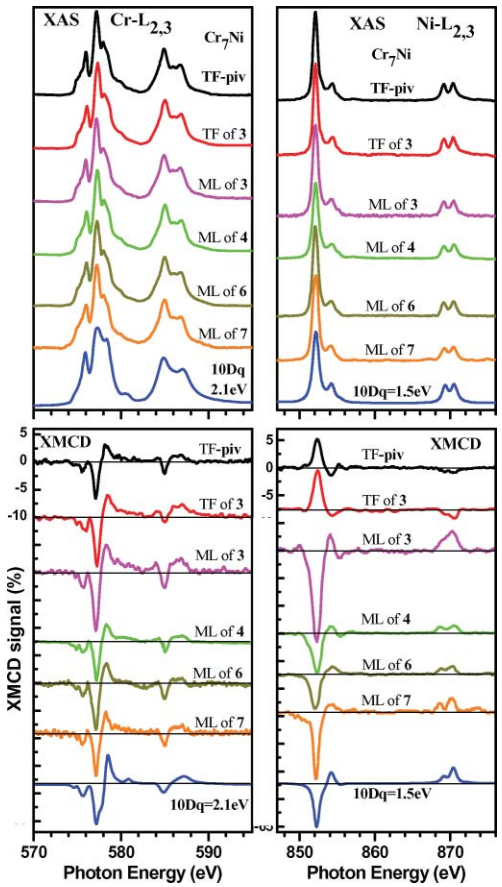

Fig. 5 Cr (Left panel) and Ni (right panel) $L_{2,3}$ XAS and XMCD spectra for the MLs of **3**, **4**, **6** and **7**, compared with the TFs of **3** and of the pristine Cr7Ni-pivalate measured at 10 K and 5T. The TT multiplet calculations (taken from ref. 22)with 10Dq = 2.1 eV for Cr^{3+} and 10Dq = 1.5 eV for Ni^{2+} are also shown.

and Ds = Dt = 0, 10Dq = 1.5 eV for Ni^{2+} (see details in ref. 22). This implies that in all the $\{Cr_7Ni\}$ systems the slightly distorted octahedral environment around the Cr and Ni ions can be safely approximated by an almost perfect octahedron.

Information on the intramolecular interactions can be extracted from the study of the sign of the dichroic signal. Indeed, when an external magnetic field is applied, a competition arises between the antiferromagnetic coupling between nearest-neighbouring ions (favouring a staggered configuration of magnetic moments at low temperature) and the Zeeman interaction tending to align the magnetic moments along the field direction. The XMCD spectra (Fig. 5) provide information on this interplay. The negative dichroic signal at the Cr-L_3 edge and the positive one at the L_2 edge [$(L3)^-$, $(L2)^+$ in short] imply that the total magnetic moment of Cr ions is parallel to **H**. This occurs for both TFs and MLs, for all the explored temperatures T and applied magnetic fields, **H**. The opposite behavior *i.e.*, [$(L3)^+$, $(L2)^-$] was observed at 10 K for Ni in every TFs measurement, implying that the expected magnetic moment is antiparallel to **H**, whereas for all the MLs the Ni magnetic moment is parallel to **H**. While the sign of the Ni dichroic signal is the same in every studied ML and opposite to that observed in bulk samples (TFs), its intensity depends on the specific derivative. From a quantitative analysis of the spectra taken on different MLs (see Fig. 5 and Tab. 3) we derived that the magnitude of the normalized Ni XMCD signal for the derivative **3** (17%) is twice respect to the value of the other derivatives. Notice that the entity of the dichroic signal is not necessarily related to the proximity of Ni to the surface (*e.g.* length of ligands). A possible cause could be the distortion of the ring with respect to the bulk conditions, due to the lack of the isotropic interactions with the surrounding molecules in a 3D crystal. The resulting change in the overlap integrals yielding the superexchange paths explains the observed decrease of exchange constants with respect to their TF values. The fact that the stronger is the ligand-substrate bonding, the higher is the measured Ni dichroic signal, suggests that the distortion of the ring is modulated by the strains due to the ligands-substrate bond.[22]

We have refined the above analysis by extracting the mean value of the spin (m_S) and orbital (m_O) magnetic moments (along the direction perpendicular to the surface) for Cr and Ni ions by using XMCD sum rules.[34,39] Fig. 6 shows the Cr-$L_{2,3}$ and Ni-$L_{2,3}$ absorption spectra taken using both photon helicities (upper panel), the relative dichroic signal and its integral (lower panel) measured for the ML of **3** at 10 K and 5T. We make use of the same analysis successfully applied to the TFs of Cr_xInNi ($x = 6,7$),[40] Cr_8, Cr_7Ni-piv,[34] and to the ML of **3**[22] (see references for more detail). Briefly, the orbital (m_O) and spin (m_S) magnetic moments can be obtained from the following expressions:

$$m_S/\mu_B = -\frac{(6p-4q)}{r}\cdot N_{eff}\cdot SC \qquad m_o/\mu_B = -\frac{4q}{3r}\cdot N_{eff}$$

where N_{eff}, the number of holes in the 3d shell, is equal to 7 and 2 for Cr^{3+} and Ni^{2+}, respectively. For Cr we used a spin correction (SC) factor of 1.75.[22,34] For all TFs and MLs investigated we observe the vanishing of the dichroic signal integral at the Cr-$L_{2,3}$ edges, that is the orbital moment of the Cr^{3+} ions is completely quenched by the crystal field. On the contrary, for Ni^{2+} ions the orbital magnetic moment derived by the sum rules is of about 10% of the spin magnetic moment (partial quenching). It follows that Cr ions have a purely spin gyromagnetic factor ($g_{Cr} = 2.0$), whereas for Ni is $g_{Ni} = 2.2 \pm 0.1$, very close to the one derived for the Cr_7Ni-piv system (see Tab. 3). We may thus conclude that neither

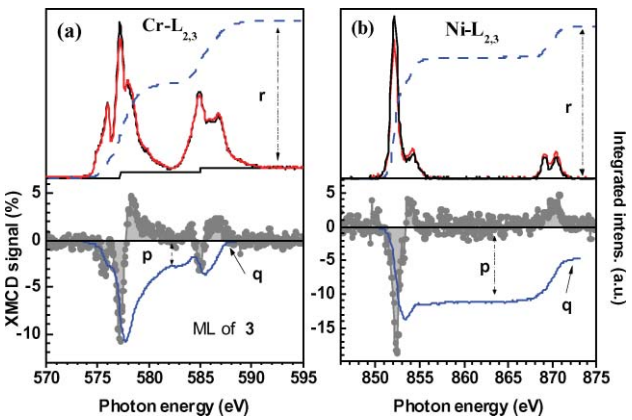

Fig. 6 Upper panels: Cr (a) and Ni (b) $L_{2,3}$ XAS spectra taken with $\sigma^{\uparrow\uparrow}$ and $\sigma^{\uparrow\downarrow}$ circularly polarized light and the XAS integral (dashed line) at 5 T and 10 K for the ML of **3**. Lower panels: XMCD ($\sigma^{\uparrow\downarrow} - \sigma^{\uparrow\uparrow}$) spectra (dotted lines) and their integrals (continuous lines). The parameters p, q and r are the values of the integrals used for the sum rules analysis.

Table 3 Intensity of the XMCD signals, measured at 10 K and 5T, at the Cr and Ni $L_{2,3}$ edges. Total magnetic moments ($m_O + m_S$) derived by sum rules for 7Cr (column 4), 1 Ni (column 7) and their sum (last column), *i.e.* the total magnetic moments of the Cr_7Ni ring. The Cr and Ni *g*-factors derived by sum rules are also shown. (*) The magnetic moments uncertainty takes into account the signal-to-noise ratio of the spectrum from which it was derived.

Derivative	g_{Cr}±0.1	XMCD Cr (%)	$m_O + m_S$ 7Cr (μ_B) ± 0.2*	g_{Ni}±0.1	XMCD Ni (%)	$m_O + m_S$ Ni (μ_B) ± 0.04*	$m_O + m_S$ Cr_7Ni (μ_B) ± 0.25*
TF-piv	2.0	6.0	0.92	2.2	–5	–0.10	0.82
TF of **3**	2.0	7.8	1.16	2.2	–6.7	–0.13	1.03
ML of **3**	2.0	10.5	1.6	2.2	18	0.37	1.97
ML of **4**	2.0	7.2	1.1	2.2	7.1	0.14	1.24
ML of **6**	2.0	8.5	1.3	2.2	6.2	0.13	1.43
ML of **7**	2.0	7.6	1.15	2.2	12	0.24	1.39

the functionalization nor the grafting onto the Au surface affects the degree of quenching of the orbital momentum.

In Table 3 the total magnetic moments are reported ($m_t = m_O + m_S$) derived by sum rules for 7 Cr ions, for one Ni and for their sum, which represents the total magnetic moments of the whole Cr_7Ni ring. If we compare the first two derivatives in Table 3, we see that the effects of the functionalization on the magnetic properties of Cr_7Ni molecules in the TF is small, because we observe only a maximum change of m_t of about 20% (derivative 3) with respect to the pristine compound Cr_7Ni-piv. This result agrees with the theoretical calculations of the exchange constants, which show a reduction of 15% when the pivalate ligand is substituted with the 3-tpc.[22] From a quantitative analysis of the different MLs (see Tab. 3) we derived for **3** a total magnetic moment ($m_t = 1.97\mu_B$), which is higher than in the non-covalent interacting derivatives **6** ($1.43\mu_B$) and **7** ($1.39\mu_B$) and twice the value relative to the TFs. On the contrary, derivative **4** with the single protected sulfur, has $m_t = 1.24\mu_B$ and is the one with the lowest ring distortion and thus the one in which the gap between the doublet ground state and the excited states is more similar to the bulk $\{Cr_7Ni\}$ ring. These results suggest that the stronger the ligand-substrate bonding, the higher the measured Ni dichroic signal, in other words the distortion of the ring is modulated by the strains due to the ligands-substrate bonding. In ref. 22 these results were compared with accurate theoretical analysis. Simulations indicate that a small reduction of the magnetic exchange constant is sufficient to account for the change in sign of the Ni magnetic moment. In agreement with the experimental results, density-functional calculations show that weak stretching of the structure of the ring give rise to perturbations of both $J_{Cr\text{–}Cr}$ and the $J_{Cr\text{–}Ni}$. The effect of the reduction of the exchange constants, in turns, is the decrease of the energy separation between the spin 1/2 ground state and the excited states.[22] While this may require lower temperatures for the inizialization of the ground state, it does not compromise the possibility of observing quantum phenomena also on isolated $\{Cr_7Ni\}$ molecules deposited on Au(111).[15–17]

Conclusions

By a systematic investigation we have shown that it is possible to obtain a 2D distribution of isolated $\{Cr_7Ni\}$ rings by exploiting the direct binding of sulfur-functionalized derivatives on a gold surface or by alternative functionalization pathways. In both these approaches, the ring stoichiometry is preserved as proved by the core level photoemission. The S 2p binding energies together with the cluster stability against the STM tip perturbation indicate a robust grafting on the Au surface for all the S-based functionalization pathways (amino-ethanethiol, thiophene, sulfur protected). In case of the S-free derivatives the coverage is still sizable (15–25%), but the bonding strength is smaller than the sulfur-functionalized derivatives, as shown by STM. The best results, *i.e.* the highest level of coverage (about 25–35%) together with bonding robustness and the smallest coverage fraction of free ligands, is achieved with the Cr_7Ni-4mtpp derivative, which grafts to the gold surface with a single protected S-atom.

For all $\{Cr_7Ni\}$ derivatives here investigated, the electronic properties (high energy scales) of molecular $\{Cr_7Ni\}$ rings are the same for thick films and sub-monolayer samples, whereas the magnetic properties (reflecting low-energy scales) are slightly different and can be influenced by the different functionalization pathways. Also in this case the Cr_7Ni-4mtpp derivative is the less perturbed when is deposited on a gold surface. These results demonstrate that these complex magnetic molecules can be safely grafted on surfaces without any drastic chemical changes, just with a small perturbation of their magnetic features, that give rise to a small reduction of exchange coupling without compromising the possibility to observe quantum phenomena. Furthermore, the peculiar properties of $\{Cr_7Ni\}$ molecules are retained when they are deposited on the Au(111) surface. These findings pave the way to the realization of hybrid systems comprising distributions of isolated $\{Cr_7Ni\}$ molecules that preserve their bulk magnetic features.

Experimental

The submonolayers (sML) were obtained by immersing the Au(111) or Au/mica flamed-annealed surface in a mM solution of the specific derivative. Tetrahydrofuran (THF) solvent was used for Cr_7Ni-thio, Cr_7Ni-thiobutane, Cr_7Ni-3tpc, Cr_7Ni-4mtpp, Cr_7Ni-pyrid; dichloromethane (DCM) solvent was used for Cr_7Ni-phenoxy and CoPc-Cr_7Ni. Scanning tunnelling microscopy (STM) and X-ray photoemission spectroscopy (XPS) were used to check that the desired two dimensional distribution of nanometric entities was actually obtained. Thick films (TFs) were obtained by drop casting the saturated solution on highly oriented pyrolytic graphite (HOPG) substrate.

STM measurements were carried out by an Omicron UHV VT-STM system. The tips used were electrochemically etched tungsten wires. Room temperature STM acquisitions were carried out in constant current mode with typical imaging conditions of 2.0 V and the lowest achievable current (30 pA) in order to minimize dragging and damaging of the soft organic materials with the scanning tip. XPS measurements were performed using an Omicron

hemispherical analyzer (EA125) and a non-monochromatized MgKα X-ray source ($h\nu = 1253.6$ eV).

XMCD experiments were carried out at the ID8 beamline of the European Synchrotron Radiation Facility (ESRF) in Grenoble (France). The lowest sample temperature reached was about 10 K and the base pressure of the experimental chamber 1.0×10^{-10} mbar. The photon source was an Apple II undulator that delivers a high flux of polarized light. We paid much attention to avoid any sample degradation induced by radiation exposure, working with very low flux (below 10^{12} photons/s) and by strictly monitoring XAS spectra throughout all the experiments for detecting even the smallest traces of sample damaging. XMCD measurements at the Cr and Ni $L_{2,3}$ edges were performed in total electron yield mode using circularly polarized light with about 100% polarization rate and with external magnetic field $\mu_0\mathbf{H}$ up to 5 T applied perpendicularly to the sample surface and parallel to the incident photon beam. The dichroic spectrum is the difference between the XAS spectra taken with the helicity of the incident photon antiparallel ($\sigma^{\uparrow\downarrow}$) and parallel ($\sigma^{\uparrow\uparrow}$) to the sample magnetization (**M**). In order to minimize the effects of field inhomogeneity, we carried out measurements by switching both the helicity and the applied field. The $\sigma^{\uparrow\uparrow}$ ($\sigma^{\uparrow\downarrow}$) absorption spectra are therefore the average spectra collected with the helicity parallel (antiparallel) to the sample magnetization.

Acknowledgements

This work was partially supported by the European project FP7-ICT FET Open "MolSpinQIP" project, contract N.211284 and by the Italian MUR through a PRIN project. We acknowledge the European Synchrotron Radiation Facility for provision of synchrotron radiation facilities and we thank Julio Criginsky Cezar, Fabrizio Moro and Valentina de Renzi for assistance during experiments at the beamline ID8. We are also grateful to the EPSRC(UK) for support, and to The Royal Society for a Wolfson Merit Award (to R. E. P. W.)

References

1 C. Joachim, J. K. Gimzewski and A. Aviram, *Nature*, 2000, **408**, 541.
2 A. Caneschi, D. Gatteschi, R. Sessoli, A. L. Barra, L. C. Brunel and M. Guillot, *J. Am. Chem. Soc.*, 1991, **113**, 5873; R. Sessoli, H. L. Tsai, A. R. Schake, S. Y. Wang, J. B. Vincent, K. Folting, D. Gatteschi, G. Christou and D. N. Hendrickson, *J. Am. Chem. Soc.*, 1993, **115**, 1804.
3 W. Wernsdorfer, N. Aliaga-Alcalde, D. N. Hendrickson and G. Christou, *Nature*, 2002, **416**, 406.
4 A. Cornia, A. C. Fabretti, M. Pacchioni, L. Zobbi, D. Bonacchi, A. Caneschi, D. Gatteschi, R. Biagi, U. del Pennino, V. De Renzi, L. Gurevich and H. S. J. Van Der Zant, *Angew. Chem., Int. Ed.*, 2003, **42**, 1645.
5 L. Bogani, L. Cavigli, M. Gurioli, R. L. Novak, M. Mannini, A. Caneschi, F. Pineider, R. Sessoli, M. Clemente-León, E. Coronado, A. Cornia and D. Gatteschi, *Adv. Mater.*, 2007, **19**, 3906.
6 M. Mannini, P. Sainctavit, R. Sessoli, C. Cartier dit Moulin, F. Pineider, M.-A. Arrio, A. Cornia and D. Gatteschi, *Chem.–Eur. J.*, 2008, **14**, 7530.
7 E. Coronado, A. Forment Aliaga, F. M. Romero, V. Corradini, R. Biagi, V. De Renzi, A. Gambardella and U. del Pennino, *Inorg. Chem.*, 2005, **44**, 7693.
8 S. Voss, M. Fonin, U. Rüdiger, M. Burgert, U. Groth and Yu. S. Dedkov, *Phys. Rev. B: Condens. Matter Mater. Phys.*, 2007, **75**, 045102.
9 S. Klyatskaya, J. R. Galan Mascaros, L. Bogani, F. Hennrich, M. Kappes, W. Wernsdorfer and M. Ruben, *J. Am. Chem. Soc.*, 2009, **131**, 15143–15151.
10 J. Gomez-Segura, I. Diez-Perez, N. Ishikawa, M. Nakano, J. Veciana and D. Ruiz-Molina, *Chem. Commun.*, 2006, 2866–2868.
11 N. Lin, S. Stepanow, M. Ruben and J. V. Barth, *Top. Curr. Chem.*, 2009, 1–44.
12 I. Salitros, N. T. Madhu, R. Boca, J. Pawlik and M. Ruben, *Monatsh. Chem.*, 2009, **140**, 695–733.
13 M. Mannini, F. Pineider, Ph. Sainctavit, C. Danieli, E. Otero, C. Sciancalepore, A. M. Talarico, M. A. Arrio, A. Cornia, D. Gatteshi and R. Sessoli, *Nat. Mater.*, 2009, **8**, 194; P. Gambardella, S. Stepanow, A. Dmitriev, J. Honolka, F. M. F. de Groot, M. Lingenfelder, S. S. Gupta, D. D. Sarma, P. Bencok, S. Stonescu, S. Clair, S. Pons, N. Lin, A. P. Seitsonen, H. Brune, J. V. Barth and K. Kern, *Nat. Mater.*, 2009, **8**, 189.
14 A. Ghirri, A. Candini, M. Evangelisti, G. C. Gazzadi, M. Affronte, F. Volatron, D. Brinzei, B. Fleury, L. Catala, C. David and T. Mallah, *Small*, 2008, **4**, 2240.
15 S. Carretta, P. Santini, G. Amoretti, M. Affronte, A. Ghirri, I. Sheikin, S. Piligkos, G. Timco and R. E. P. Winpenny, *Phys. Rev. B: Condens. Matter Mater. Phys.*, 2005, **72**, 060403; S. Carretta, P. Santini, G. Amoretti, T. Guidi, J. R. D. Copley, Y. Qiu, R. Caciuffo, G. Timco and R. E. P. Winpenny, *Phys. Rev. Lett.*, 2007, **98**, 167401.
16 S. Carretta, P. Santini, G. Amoretti, M. Affronte, A. Ghirri, I. Sheikin, S. Piligkos, G. A. Timco and R. E. P. Winpenny, *Phys. Rev. B: Condens. Matter Mater. Phys.*, 2005, **72**, 060403; S. G. A. Timco, S. Carretta, F. Troiani, F. Tuna, R. J. Pritchard, E. J. L. McInnes, A. Ghirri, A. Candini, P. Santini, G. Amoretti, M. Affronte and R. E. P. Winpenny, *Nat. Nanotechnol.*, 2009, **4**, 173.
17 A. Candini, G. Lorusso, F. Troiani, A. Ghirri, S. Carretta, P. Santini, G. Amoretti, C. Muryn, F. Tuna, G. Timco, E. J. L. McInnes, R. E. P. Winpenny, W. Wernsdorfer and M. Affronte, *Phys. Rev. Lett.*, 2010, **104**, 037203.
18 F. Troiani, A. Ghirri, M. Affronte, S. Carretta, P. Santini, G. Amoretti, S. Piligkos, G. Timco and R. E. P. Winpenny, *Phys. Rev. Lett.*, 2005, **94**, 207208; F. Troiani, M. Affronte, S. Carretta, P. Santini and G. Amoretti, *Phys. Rev. Lett.*, 2005, **94**, 190501.
19 F. K. Larsen, E. J. L. McInnes, H. El Mkami, J. Overgaard, S. Piligkos, G. Rajaraman, E. Rentschler, A. A. Smith, G. M. Smith, V. Boote, M. Jennings, G. A. Timco and R. E. P. Winpenny, *Angew. Chem., Int. Ed.*, 2003, **42**, 101.
20 M. Affronte, F. Troiani, A. Ghirri, S. Carretta, P. Santini, V. Corradini, R. Schuecker, C. Muryn, G. A. Timco and R. E. P. Winpenny, *Dalton Trans.*, 2006, 2810.
21 V. Corradini, R. Biagi, U. del Pennino, V. De Renzi, A. Gambardella, M. Affronte, C. A. Muryn, G. A. Timco and R. E. P. Winpenny, *Inorg. Chem.*, 2007, **46**, 4937.
22 V. Corradini, F. Moro, R. Biagi, V. De Renzi, U. del Pennino, V. Bellini, S. Carretta, P. Santini, V. A. Milway, G. A. Timco, R. E. P. Winpenny and M. Affronte, *Phys. Rev. B: Condens. Matter Mater. Phys.*, 2009, **79**, 144419, and selected for the April 27, 2009 issue of *Virtual Journal of Nanoscale Science & Technology*.
23 M. Affronte, F. Troiani, A. Ghirri, A. Candini, M. Evangelisti, V. Corradini, S. Carretta, P. Santini, G. Timco and R. E. P. Winpenny, *J. Phys. D: Appl. Phys.*, 2007, **40**, 2999.
24 G. E. Poirier, *Langmuir*, 1997, **13**, 2019; G. Yang and G. Liu, *J. Phys. Chem. B*, 2003, **107**, 8746.
25 M. J. Esplandiù, H. Hagenstrom and D. M. Kolb, *Langmuir*, 2001, **17**, 828.
26 J. Noh, E. Ito, K. Nakajima, J. Kim, H. Lee and M. Hara, *J. Phys. Chem. B*, 2002, **106**, 7139.
27 J. Noh, E. Ito, T. Araki and M. Hara, *Surf. Sci.*, 2003, **532–535**, 1116.
28 D. G. Castner, K. Hinds and D. W. Grainger, *Langmuir*, 1996, **12**, 5083.
29 T. Ishida, N. Choi, W. Mizutani, H. Tokumoto, I. Kojima, H. Azehara, H. Hokari, U. Akiba and M. Fujihira, *Langmuir*, 1999, **15**, 6799; T. Ishida, M. Hara, I. Kojima, S. Tsuneda, N. Nishida, H. Sasabe and W. Knoll, *Langmuir*, 1998, **14**, 2092.
30 C. Vericat, M. E. Vela, G. Andreasen, R. C. Salvarezza, L. Vazquez and J. A. Martın-Gago, *Langmuir*, 2001, **17**, 4919; G. Liu, J. A. Rodriguez, J. Dvorak, J. Hrbek and T. Jirsak, *Surf. Sci.*, 2002, **505**, 295.
31 E. O. Sako, H. Kondoh, I. Nakai, A. Nambu, T. Nakamura and T. Ohta, *Chem. Phys. Lett.*, 2005, **413**, 267.
32 M. Affronte, I. Casson, M. Evangelisti, A. Candini, S. Carretta, C. A. Muryn, S. J. Teat, G. A. Timco, W. Wernsdorfer and R. E. P. Winpenny, *Angew. Chem., Int. Ed.*, 2005, **44**, 6496.

33 Xing Lu *et al.*, *J. Am. Chem. Soc.*, 1996, **118**, 7197; C. Ludwig *et al.*, *J. Vac. Sci. Technol., B*, 1994, **12**, 1963.
34 V. Corradini, F. Moro, R. Biagi, U. del Pennino, V. De Renzi, S. Carretta, P. Santini, M. Affronte, J. C. Cezar, G. A. Timco and R. E. P. Winpenny, *Phys. Rev. B: Condens. Matter Mater. Phys.*, 2008, **77**, 014402, and selected for the January 14, 2008 issue of *Virtual Journal of Nanoscale Science & Technology*.
35 E. Gaudry, P. Sainctavit, F. Juillot, F. Bondioli, P. Ohresser and I. Letard, *Phys. Chem. Miner.*, 2006, **32**, 710.
36 M.-A. Arrio, A. Scuiller, P. Sainctavit, C. Cartier dit Moulin, T. Mallah and M. Verdaguer, *J. Am. Chem. Soc.*, 1999, **121**, 6414.
37 B. T. Thole, G. Van Der Laan, J. C. Fuggle, G. A. Sawatzky, R. C. Karnatak and J. M. Esteva, *Phys. Rev. B: Condens. Matter*, 1985, **32**, 5107; B. T. Thole, G. Van Der Laan and P. H. Butler, *Chem. Phys. Lett.*, 1988, **149**, 295.
38 F. M. F. de Groot, *J. Electron Spectrosc. Relat. Phenom.*, 1994, **67**, 529; F. M. F. de Groot, *Chem. Rev.*, 2001, **101**, 1779.
39 C. T. Chen, Y. U. Idzerda, H. J. Lin, N. V. Smith, G. Meigs, E. Chaban, G. H. Ho, E. Pellegrin and F. Sette, *Phys. Rev. Lett.*, 1995, **75**, 152.
40 A. Ghirri, G. Lorusso, F. Moro, F. Troiani, V. Corradini, C. Muryn, F. Tuna, G. Timco, R. E. P. Winpenny and M. Affronte, *Phys. Rev. B: Condens. Matter Mater. Phys.*, 2009, **79**, 224430.

